

A nontopological soliton with a dipole chromomagnetic field

A. Yu. Loginov^{1,*}

¹*Laboratory of Applied Mathematics and Theoretical Physics,
Tomsk State University of Control Systems and Radioelectronics, 634050 Tomsk, Russia*

(Dated: June 26, 2025)

A non-Abelian gauge model with a complex isovector scalar field and a sixth-order self-interaction potential is considered. It is shown that it has a nontopological soliton solution. The features of this soliton include a monopole-like core surrounded by a Q-ball-like shell, the existence of radially excited states, and a long-range dipole chromomagnetic field. The properties of the soliton are studied using analytical and numerical methods. In particular, the asymptotic dependencies of the energy and the Noether charge on a phase frequency are obtained for two extreme regimes. It is also found that in these two extreme regimes, the chromomagnetic dipole moment of the soliton is proportional to its linear size.

I. INTRODUCTION

Topological and nontopological solitons [1–3] play an important role in mathematical physics, high-energy physics, condensed matter physics, cosmology, and hydrodynamics. The 't Hooft-Polyakov monopole [4, 5] is a three-dimensional topological soliton of exceptional importance in field theory. A classical model of field theory that admits the existence of the 't Hooft-Polyakov monopole is the $SU(2)$ Georgi-Glashow model [6]. It includes a real isovector scalar field ϕ that interacts minimally with a non-Abelian gauge field. The fourth-order self-interaction potential of this model has a two-dimensional sphere $|\phi| = \phi_{\text{vac}}$ as the true vacuum manifold. The potential has no false vacuum points, and, in particular, the zero point $\phi = 0$ is its local maximum.

The model of [6] can be modified in several ways. For example, the self-interaction potential can be changed so that it will have both a global minimum (true vacuum) and a local minimum (false vacuum). In particular, the potential of the model considered in [7, 8] has the zero point $\phi = 0$ as the true vacuum, and the two-dimensional sphere $|\phi| = \phi_{\text{vac}}$ as the false vacuum manifold. This model possesses metastable monopole solutions, which interpolate between the true and false vacua. Monopole solutions of this type can significantly increase the decay rate of the false vacuum [7–12].

In contrast to [7, 8], the potential of the model considered in [13] has the two-dimensional sphere $|\phi| = \phi_{\text{vac}}$ as the true vacuum manifold and the zero point $\phi = 0$ as the false vacuum. It has been shown in [13] that this model has a solution, which consists of a monopole-like core surrounded by a region (bubble) of the true vacuum. Being a stationary point of an Euclidean action, this gauged monopole-bubble contributes to the decay amplitude of the false vacuum in the high-temperature limit.

A classical example of a solution, which is a stationary point of an Euclidean action is the bounce. A solution of this type was first described in [14] in the framework

of the model of a self-interacting real scalar field in Euclidean space. The bounce determines the decay amplitude of a false vacuum in the semiclassical approximation. There is another solution of field theory called the Q-ball [15], which is closely related to the bounce solution [14]. The Q-ball is a time-dependent nontopological soliton of the model of a self-interacting complex scalar field in Minkowski space. The Q-ball is a stationary point of the energy functional at a fixed Noether charge. The complex scalar field of the model results in the Noether charge, which is necessary for the existence of the Q-ball.

In this paper, we consider a non-Abelian gauge model with a complex isovector scalar field and a sixth-order self-interaction potential. This model allows the existence of a nontopological soliton. This soliton is related to the gauged monopole-bubble [13] similar to how the Q-ball and the bounce are related. The nontopological soliton of the model consists of a monopole-like core surrounded by a shell of the Q-ball type. Like the usual Q-ball, this shell can be either in the ground state or in a radially excited state. The energy and the Noether charge of the soliton depend on a phase frequency, which determines the time dependence of the complex isovector scalar field. A characteristic feature of the soliton is its long-range chromomagnetic field of the dipole type. At the same time, the soliton does not possess any electric field.

This paper is structured as follows. In Sec. II, we describe briefly the Lagrangian, symmetries, and field equations of the model under consideration. In Sec. III, the general properties of the nontopological soliton are considered and discussed. In particular, we derive two basic relations which determine the properties of the soliton. In Sec. IV, we study the behavior of the nontopological soliton in two (thin-wall and thick-wall) extreme regimes. In Sec. V, we present and discuss numerical results. In the final section, we briefly summarize the results obtained in this paper.

Throughout the paper, the natural units $c = 1$ and $\hbar = 1$ are used.

* a.yu.loginov@tusur.ru

II. THE LAGRANGIAN AND FIELD EQUATIONS OF THE MODEL

The Lagrangian density of the model considered here has the form

$$\mathcal{L} = -\frac{1}{4}F_{\mu\nu}^a F^{a\mu\nu} + D_\mu\phi^a D^\mu\phi^{a*} - V(\phi^a\phi^{a*}), \quad (1)$$

where

$$F_{\mu\nu}^a = \partial_\mu A_\nu^a - \partial_\nu A_\mu^a - g\epsilon^{abc}A_\mu^b A_\nu^c \quad (2)$$

is the non-Abelian field strength,

$$D_\mu\phi^a = \partial_\mu\phi^a - g\epsilon^{abc}A_\mu^b\phi^c \quad (3)$$

is the covariant derivative of the complex isovector scalar field ϕ , and

$$V(\phi^a\phi^{a*}) = \frac{m^2\phi^a\phi^{a*}}{1+\varepsilon^2} \left[\left(1 - \frac{\phi^a\phi^{a*}}{v^2}\right)^2 + \varepsilon^2 \right] \quad (4)$$

is the sixth-order self-interaction potential. This form of writing the potential was used in [3] in the context of Q-balls; its advantage is that it has a zero global minimum at $\phi = 0$ for any values of the parameters m , v , and ε . Hence, the $SU(2)$ gauge symmetry of the model (1) cannot be spontaneously broken.

Using standard methods of field theory, we obtain the field equations of the model:

$$\begin{aligned} D_\nu F^{a\mu\nu} + g\epsilon^{abc}[\phi^b(D^\mu\phi^c)^* + \phi^{b*}D^\mu\phi^c] &= 0, \quad (5) \\ D_\mu D^\mu\phi^a + V'(\phi^a\phi^{a*})\phi^a &= 0, \quad (6) \end{aligned}$$

where

$$V'(\phi^a\phi^{a*}) = m^2 - \frac{4m^2\phi^a\phi^{a*}}{v^2(1+\varepsilon^2)} + \frac{3m^2(\phi^a\phi^{a*})^2}{v^4(1+\varepsilon^2)} \quad (7)$$

is the derivative of the potential (4) with respect to the sesquilinear combination $\phi^a\phi^{a*}$. We will also need the expression of the energy-momentum tensor of the model,

$$\begin{aligned} T_{\mu\nu} &= -F_{\mu\rho}^a F_\nu^{a\rho} + D_\mu\phi^a D_\nu\phi^{a*} + D_\nu\phi^a D_\mu\phi^{a*} \quad (8) \\ &+ \eta_{\mu\nu} \left[\frac{1}{4}F_{\rho\tau}^a F^{a\rho\tau} - D_\rho\phi^a D^\rho\phi^{a*} + V(\phi^a\phi^{a*}) \right]. \end{aligned}$$

Besides the local gauge $SU(2)$ transformations, the Lagrangian (1) is also invariant under the global $U(1)$ transformations

$$\phi^a \rightarrow e^{i\chi}\phi^a, \quad \phi^{a*} \rightarrow e^{-i\chi}\phi^{a*}. \quad (9)$$

The corresponding conserved Noether current is

$$j^\mu = i(\phi^a D^\mu\phi^{a*} - \phi^{a*} D^\mu\phi^a). \quad (10)$$

Note that the current (10) is invariant under both the local gauge $SU(2)$ transformations and the global $U(1)$ transformations.

The model (1) differs from the well-known $SU(2)$ Georgi-Glashow model [6] in several important respects. The model (1) contains the complex isovector scalar field ϕ , whereas the $SU(2)$ Georgi-Glashow model contains a real isovector scalar field. Further, the sixth-order potential (4) has a zero global minimum at the zero point $\phi = 0$, and therefore the classical vacuum does not break the gauge $SU(2)$ symmetry. In contrast, the fourth-order potential of the Georgi-Glashow model reaches a zero minimum on a two-dimensional sphere $|\phi| = \phi_{\text{vac}}$ resulting in a spontaneous breaking of the gauge $SU(2)$ symmetry.

III. THE SOLITON SOLUTION AND ITS PROPERTIES

To find a soliton solution of the model (1), we shall use a modified 't Hooft-Polyakov ansatz

$$A^{a0} = vj(r)n^a, \quad (11)$$

$$A^{ai} = \epsilon^{aim}n^m \frac{1-u(r)}{gr}, \quad (12)$$

$$\phi^a = 2^{-1/2}vh(r)e^{i\omega t}n^a, \quad (13)$$

where $n^a = x^a/r$. The modification consists in the time dependence $\propto e^{i\omega t}$ of the complex isovector scalar field in Eq. (13). This time dependence is typical for nontopological soliton solutions [3, 15, 16]. Substituting Eqs. (11)–(13) into the field equations (5)–(6), we obtain a system of nonlinear differential equations for the ansatz functions:

$$j''(r) + \frac{2}{r}j'(r) - \frac{2}{r^2}u(r)^2j(r) = 0, \quad (14)$$

$$\begin{aligned} u''(r) - \frac{1}{r^2}u(r)(u(r)^2 - 1) \\ - \frac{m_V^2}{2}(h(r)^2 - j(r)^2)u(r) = 0, \quad (15) \end{aligned}$$

$$\begin{aligned} h''(r) + \frac{2}{r}h'(r) - \frac{2}{r^2}u(r)^2h(r) \\ + m^2\partial\tilde{U}_\omega(h(r))/\partial h = 0, \quad (16) \end{aligned}$$

where

$$\tilde{U}_\omega(h) = -\frac{1}{2} \left(\frac{m_\omega^2}{m^2}h^2 - \frac{h^4}{1+\varepsilon^2} + \frac{1}{4} \frac{h^6}{1+\varepsilon^2} \right) \quad (17)$$

is a dimensionless effective potential, $m_V = \sqrt{2}gv$ is the mass of the gauge vector boson, and $m_\omega = (m^2 - \omega^2)^{1/2}$ is an effective ω -dependent mass parameter.

It follows from Eqs. (4) and (13) that the potential (4) vanishes only at zeros of the ansatz function $h(r)$. Then, from the condition of the finiteness of the soliton's energy, it follows that $\lim_{r \rightarrow \infty} h(r) = 0$. Hence, we can neglect the terms $-m_V^2 h^2 u/2$ and $-u(u^2 - 1)/r^2$ as $r \rightarrow \infty$, and Eq. (15) takes the asymptotic form

$$u''(r) + \frac{m_V^2}{2}j(r)^2u(r) = 0. \quad (18)$$

Eq. (18) tells us that if $\lim_{r \rightarrow \infty} j(r) \equiv j_\infty \neq 0$, then the ansatz function $u(r)$ will oscillate at large r , which is incompatible with the finiteness of the energy of the soliton solution. We thus conclude that the limiting value $j_\infty = 0$.

Further, Eq. (11) tells us that the regularity of the solution at the origin leads to another boundary condition $j(0) = 0$, so that $j(r)$ vanishes at these two boundary points. To satisfy these homogeneous boundary conditions, the positive (negative) ansatz function $j(r)$ must reach a global maximum (minimum) at some point $r = \bar{r}$. In other words, the relation $\text{sgn}(j''(\bar{r})) = -\text{sgn}(j(\bar{r}))$ must hold at this point. However, it follows from Eq. (14) that $j''(\bar{r}) = 2u(\bar{r})^2 j(\bar{r})/\bar{r}^2$, and hence $\text{sgn}(j''(\bar{r})) = \text{sgn}(j(\bar{r}))$. It follows from the contradiction obtained that

$$j(r) = 0. \quad (19)$$

We see that a finite energy soliton solution cannot possess an electric field, and hence an electric charge.

Using Eqs. (8), (12), and (13), we obtain the expression for the energy of the soliton solution in terms of the ansatz functions $u(r)$ and $h(r)$

$$E = 4\pi v^2 \int_0^\infty \left[\frac{\omega^2}{2} h(r)^2 + \frac{2u'(r)^2}{m_V^2 r^2} + \frac{(u(r)^2 - 1)^2}{m_V^2 r^4} \right. \\ \left. + \frac{1}{2} h'(r)^2 + \frac{h(r)^2 u(r)^2}{r^2} + m^2 \tilde{V}(h(r)) \right] r^2 dr, \quad (20)$$

where the dimensionless self-interaction potential is

$$\tilde{V}(h) = \frac{1}{2} \left(h^2 - \frac{h^4}{1 + \varepsilon^2} + \frac{1}{4} \frac{h^6}{1 + \varepsilon^2} \right). \quad (21)$$

Similarly, we obtain the expression for the soliton's Noether charge

$$Q = 4\pi v^2 \omega \int_0^\infty h(r)^2 r^2 dr. \quad (22)$$

We also need the expression for the soliton's chromomagnetic field $B^{ai} = -\epsilon^{ijk} F^{ajk}/2$ in terms of the ansatz functions

$$B^{ai} = \frac{u'(r)}{gr} (\delta^{ai} - n^a n^i) - \frac{1 - u(r)^2}{gr^2} n^a n^i. \quad (23)$$

We now investigate the asymptotics of the ansatz functions $u(r)$ and $h(r)$. Substituting the power expansions of these functions in Eqs. (12) and (13), we get the small r asymptotics

$$u(r) \sim 1 + \frac{u_2}{2!} r^2 + \frac{u_4}{4!} r^4 + O(r^6), \quad (24)$$

$$h(r) \sim h_1 r + \frac{h_3}{3!} r^3 + O(r^5), \quad (25)$$

where the next-to-leading expansion coefficients are

$$u_4 = \frac{3}{5} (3u_2^2 + 2m_V^2 h_1^2), \quad (26)$$

$$h_3 = \frac{3}{5} h_1 (m_\omega^2 + 2u_2). \quad (27)$$

It follows from Eqs. (24)–(25) that $u(r)$ and $h(r)$ are even and odd functions of r , respectively.

Next, we investigate the large r asymptotics of $u(r)$. We first note that $u(r)$ tends to some constant u_∞ as $r \rightarrow \infty$, otherwise the energy (20) would be infinite. It follows that at large r , the ansatz function $u(r)$ can be written as $u(r) = u_\infty + \delta(r)$, where $\delta(r) \ll 1$. Furthermore, Eq. (16) tells us that $h(r)$ tends to zero exponentially as $r \rightarrow \infty$, provided that $u(r)$ tends to a constant u_∞ . Taking this into account, we obtain the asymptotic form of Eq. (15) in terms of $\delta(r)$

$$\delta''(r) + \frac{1 - 3u_\infty^2}{r^2} \delta(r) + \frac{u_\infty (1 - u_\infty^2)}{r^2} = 0, \quad (28)$$

where we neglect terms nonlinear in δ because of their smallness in comparison with the linear term.

The solution to Eq. (28) is

$$\delta(r) = \frac{u_\infty (u_\infty^2 - 1)}{1 - 3u_\infty^2} + b_1 r^{\alpha_1} + b_2 r^{\alpha_2}. \quad (29)$$

where the exponents

$$\alpha_{1,2} = \frac{1}{2} (1 \pm i\sqrt{3(1 - 4u_\infty^2)}). \quad (30)$$

In Eq. (29), the inhomogeneous term must vanish, since $\delta(r) \rightarrow 0$ as $r \rightarrow \infty$, which leads to the following alternatives:

$$u_\infty = 0, \quad \alpha_{1,2} = \frac{1}{2} (1 \pm i\sqrt{3}) \quad (31)$$

or

$$u_\infty = \pm 1, \quad \alpha_1 = -1, \quad \alpha_2 = 2. \quad (32)$$

The first alternative corresponds to an oscillating solution with an increasing amplitude and is, therefore, unacceptable. We are left with the second option in which we choose the upper sign, since the regularity at the origin results in the boundary condition $u(0) = 1$. Thus, we have the following large r asymptotics of $u(r)$

$$u(r) \sim 1 + br^{-1} + O(r^{-2}), \quad (33)$$

where b is a constant.

Using Eq. (15), it is easy to show that $u(r)$ cannot exceed unity, since otherwise it would increase without bound. It follows that in Eq. (33), b is negative as well as u_2 in Eq. (24). Taking into account that the limit value $u_\infty = 1$ and using Eq. (16), we finally obtain the large r asymptotics of $h(r)$:

$$h(r) \sim \frac{e^{-m_\omega r}}{m_\omega r} \left[1 + \frac{1}{m_\omega r} + O(m_\omega^{-2} r^{-2}) \right]. \quad (34)$$

Comparing Eqs. (33) and (34), we see that as $r \rightarrow \infty$, $u(r)$ has long-range asymptotics $\propto r^{-1}$, whereas $h(r)$ has short-range exponential asymptotics.

Combining Eqs. (12) and (33), we obtain the large r asymptotics of the gauge field

$$A^{ai} \sim -\epsilon^{aim} n^m \frac{b}{gr^2}. \quad (35)$$

Eq. (35) tells us that the soliton has a long-range gauge field of dipole type. Indeed, Eq. (35) can be rewritten as

$$\mathbf{A}^a \sim \frac{1}{4\pi} \frac{\mathbf{m}^a \times \mathbf{r}}{r^3}, \quad (36)$$

where

$$m^{ai} = \frac{4\pi}{g} b \delta^{ai}. \quad (37)$$

Eq. (36) coincides with the expression for the vector potential of a chromomagnetic dipole with the dipole moment (37). Eqs. (23) and (33) lead to the asymptotics of the soliton's chromomagnetic field

$$B^{ai} \sim -\frac{b}{gr^3} (\delta^{ai} - n^a n^i) + \frac{2b}{gr^3} n^a n^i, \quad (38)$$

or, in vector form,

$$\mathbf{B}^a \sim \frac{1}{4\pi r^3} [3\mathbf{n}(\mathbf{m}^a \cdot \mathbf{n}) - \mathbf{m}^a]. \quad (39)$$

The soliton's energy (20) can be written as the sum of four terms

$$E = E^{(T)} + E^{(B)} + E^{(G)} + E^{(P)}, \quad (40)$$

where

$$E^{(T)} = 4\pi v^2 \int_0^\infty \frac{\omega^2}{2} h(r)^2 r^2 dr \quad (41)$$

is the kinetic part of the energy,

$$E^{(B)} = \frac{4\pi}{g^2} \int_0^\infty \left[\frac{u'(r)^2}{r^2} + \frac{(u(r)^2 - 1)^2}{2r^4} \right] r^2 dr \quad (42)$$

is the energy of the chromomagnetic field,

$$E^{(G)} = 4\pi v^2 \int_0^\infty \left[\frac{1}{2} h'(r)^2 + \frac{h(r)^2 u(r)^2}{r^2} \right] r^2 dr \quad (43)$$

is the gradient part of the energy, and

$$E^{(P)} = 4\pi v^2 \int_0^\infty m^2 \tilde{V}(h(r)) r^2 dr \quad (44)$$

is the potential part of the energy. The Lagrangian $L = \int \mathcal{L} d^3x$ can also be expressed as a linear combination of these four terms:

$$L = E^{(T)} - E^{(B)} - E^{(G)} - E^{(P)}. \quad (45)$$

Furthermore, these four terms are related by one more linear (virial) relation

$$3E^{(T)} + E^{(B)} - E^{(G)} - 3E^{(P)} = 0. \quad (46)$$

To derive Eq. (46), we need to remember that the soliton solution is an extremum of the action $S = \int_0^T \int \mathcal{L} d^3x dt$. It follows from Eqs. (41)–(45) that the Lagrangian density (1) is time-independent, which implies that $S = LT$. Hence, the soliton solution is also an extremum of the Lagrangian $L = \int \mathcal{L} d^3x$.

After the scale transformation $r \rightarrow \varkappa r$ of the argument of the ansatz functions $u(r)$ and $h(r)$ of the soliton solution, the Lagrangian L becomes a function of the scale parameter \varkappa . Since the function $L(\varkappa)$ has a stationary point at $\varkappa = 1$, its derivative vanishes at this point: $dL/d\varkappa|_{\varkappa=1} = 0$. It can easily be shown that under the rescaling $r \rightarrow \varkappa r$, $E^{(T)} \rightarrow \varkappa^{-3} E^{(T)}$, $E^{(B)} \rightarrow \varkappa E^{(B)}$, $E^{(G)} \rightarrow \varkappa^{-1} E^{(G)}$, and $E^{(P)} \rightarrow \varkappa^{-3} E^{(P)}$. Using these transformation rules and Eqs. (41)–(45), we obtain the virial relation (46).

Using Eqs. (20), (22), and (45), it is easy to show that the energy, the Lagrangian, and the Noether charge of the soliton are connected by the linear relation

$$L = \omega Q - E. \quad (47)$$

Since the soliton solution is an extremum of the Lagrangian L , the following variational relation must hold

$$\delta L = \omega \delta Q - \delta E = 0. \quad (48)$$

Eq. (48) tells us that the soliton solution is an extremum of the energy functional E among the field configurations of the Noether charge Q . Thus, the soliton solution is not only an unconditional extremum of the Lagrangian, but also a conditional extremum of the energy.

In Eq. (48), the phase frequency ω plays the role of the Lagrange multiplier, and therefore variations of the fields are arbitrary. In particular, these variations can link two infinitesimally close soliton solutions. In this case, Eq. (48) leads to the important differential relation

$$dE/dQ = \omega, \quad (49)$$

which relates the derivative of the soliton's energy with respect to the Noether charge with the phase frequency ω . Note that a similar differential relation also holds for electrically charged topological solitons [17, 18].

IV. EXTREME REGIMES OF THE SOLITON

The phase frequency ω of the complex isovector scalar field ϕ is the most important parameter; it determines

the basic properties of the soliton. The phase frequency may vary only in a limited region. It follows from Eq. (34) that $|\omega| < m$. Otherwise, the parameter $m_\omega = (m^2 - \omega^2)^{1/2}$ is purely imaginary, the asymptotics (34) is oscillatory, and the soliton's energy (20) is infinite.

Also, the magnitude of the phase frequency must be greater than some minimum value $|\omega| > \omega_{\min}$, because the soliton solution does not exist otherwise. A qualitative analysis of the differential equation (16) based on a mechanical analogy [14] shows that in order for a soliton solution to exist, the effective potential (17) must have a non-negative maximum at some nonzero h . It is easy to show that this is only possible if $|\omega| > \omega_{\min} = m\varepsilon(1 + \varepsilon^2)^{-1/2}$. We conclude that the soliton may exist, provided that

$$m\varepsilon(1 + \varepsilon^2)^{-1/2} < |\omega| < m. \quad (50)$$

A. The thin-wall regime

The thin-wall regime corresponds to a situation in which $|\omega| \rightarrow \omega_{\min} = m\varepsilon(1 + \varepsilon^2)^{-1/2}$. An analysis based on the mechanical analogy [14] reveals that in this regime, the soliton can be divided into three regions. In the inner region $r < R_c$, we approximate the ansatz functions by the first terms of their power expansions (24) and (25)

$$u(r) = 1 - r^2 R_c^{-2}, \quad (51)$$

$$h(r) = (2^{1/2} - s)r R_c^{-1}. \quad (52)$$

In Eq. (52), $2^{1/2}$ is the value of h at which the effective potential $\tilde{U}_{\omega_{\min}}(h)$ in Eq. (17) reaches a zero maximum, and the value of the parameter s is assumed to be small. Substituting Eqs. (51) and (52) into Eq. (45), we obtain the contribution of the inner region to the Lagrangian

$$L_1 = \frac{a_{-1}}{R_c} + a_1 R_c + a_3 R_c^3, \quad (53)$$

where the coefficients satisfy

$$a_{-1} = -\frac{234}{35} \frac{\pi}{g^2}, \quad (54)$$

$$a_1 \approx -\frac{34}{35} \pi (2 - 2\sqrt{2}s)v^2, \quad (55)$$

$$a_3 \approx \frac{4}{315} \pi v^2 \left(\frac{55m^2}{1 + \varepsilon^2} - 63m_\omega^2 \right) + 4\sqrt{2}\pi v^2 \left(\frac{21}{105} m_\omega^2 - \frac{25m^2}{105(1 + \varepsilon^2)} \right) s, \quad (56)$$

and we hold the terms up to the first order in s .

In the intermediate region $R_c < r < R$, we approximate the ansatz functions by

$$u(r) = 0, \quad (57)$$

$$h(r) = 2^{1/2} - s. \quad (58)$$

Using Eqs. (57) and (58), we obtain the contribution of the intermediate region to the Lagrangian

$$L_2 = \frac{4}{3} \pi v^2 (R^3 - R_c^3) \left(\Omega^2 - \sqrt{2}\Omega^2 s - 2^{-1}\mu^2 s^2 \right), \quad (59)$$

where

$$\Omega^2 = \omega^2 - \omega_{\min}^2 \quad (60)$$

and

$$\mu^2 \approx -d^2 \tilde{U}_{\omega_{\min}}(h) / dh^2 \Big|_{h=\sqrt{2}} = 4m^2 (1 + \varepsilon^2)^{-1}. \quad (61)$$

We now turn to the third (outer) region $r > R$. We assume that R is large enough to fulfill the conditions $m_V R \gg 1$ and $m_\omega R \gg 1$. Then we can neglect the terms $\propto r^{-1}$ and $\propto r^{-2}$ in Eq. (16), which allows us to lower its order by one resulting in the first-order equation

$$h' = -m \sqrt{2 |\tilde{U}_{\omega_{\min}}(h)|}. \quad (62)$$

Using Eqs. (45) and (62), it can be shown that in the leading order in R , the contribution of the outer region to the Lagrangian is

$$L_3 = -4\pi R^2 T, \quad (63)$$

where the surface tension

$$T \approx m v^2 \int_0^{\sqrt{2}} \sqrt{2 |\tilde{U}_{\omega_{\min}}(h)|} dh = \frac{m v^2}{2\sqrt{1 + \varepsilon^2}}. \quad (64)$$

Note that the contribution of the magnetic field of the outer region to L_3 is $\propto R^{-1}$, and therefore can be neglected in the limit of large R .

The Lagrangian of the soliton configuration is $L = L_1 + L_2 + L_3$, and is a function of three parameters: $L = L(R_c, R, s)$. The soliton solution is an extremum of the Lagrangian, which leads us to a system of three nonlinear equations

$$\partial_{R_c} L = 0, \quad \partial_R L = 0, \quad \partial_s L = 0. \quad (65)$$

In the leading order in the small parameter $\Omega^2 = \omega^2 - \omega_{\min}^2$, the solution of the system (65) is

$$R_c \approx \frac{\sqrt{3}}{4m} \left\{ [(1 + \varepsilon^2) (289(1 + \varepsilon^2) + 1248(m/m_V)^2)]^{1/2} - 17(1 + \varepsilon^2) \right\}^{1/2}, \quad (66)$$

$$s \approx -\sqrt{2}\Omega^2 \mu^{-2}, \quad (67)$$

and

$$R \approx \frac{2T}{\Omega^2 (\Omega^2 + \mu^2)} \frac{\mu^2}{v^2} \approx \frac{2T}{v^2 \Omega^2} = \frac{2T}{v^2 (\omega^2 - \omega_{\min}^2)}. \quad (68)$$

Substituting Eqs. (66) – (68) into the Lagrangian $L(R_c, R, s)$ and keeping the higher order terms in R , we

obtain the Lagrangian of the soliton solution as a function of the phase frequency ω

$$L(\omega) \approx -\frac{16\pi T^3 \mu^4}{3v^4 \Omega^4 (\Omega^2 + \mu^2)^2}, \quad (69)$$

where $\Omega^2 = \omega^2 - \omega_{\min}^2$.

From Eqs. (47), (49), and (69), it follows that the energy $E(Q)$ and the Lagrangian $L(\omega)$ of the soliton solution are related through the Legendre transformation $E(Q) = \omega Q - L(\omega)$. Using the known properties of the Legendre transformation, we obtain successively the expressions of the Noether charge and the energy of the soliton in the thin-wall approximation

$$Q(\omega) = \frac{dL}{d\omega} = \frac{64\pi T^3}{3v^4} \frac{\omega}{(\omega^2 - \omega_{\min}^2)^3} \quad (70)$$

and $E(Q) = E(\omega(Q))$, where

$$E(\omega) = \omega \frac{dL}{d\omega} - L(\omega) = \frac{16\pi T^3}{3v^4} \frac{5\omega^2 - \omega_{\min}^2}{(\omega^2 - \omega_{\min}^2)^3} \quad (71)$$

and the dependence $\omega(Q)$ is determined from Eq. (70). Using Eqs. (70) and (71), we find that in the thin-wall regime, the ratio E/Q is

$$\frac{E}{Q} = \omega \left(\frac{5}{4} - \frac{\omega_{\min}^2}{4\omega^2} \right), \quad (72)$$

and the derivative dE/dQ is

$$\frac{dE}{dQ} = \frac{dE/d\omega}{dQ/d\omega} = \omega. \quad (73)$$

We see that both $E/|Q|$ and $dE/d|Q|$ tend to the same limit $\omega_{\min} = m\varepsilon(1 + \varepsilon^2)^{-1/2}$ as $|\omega| \rightarrow \omega_{\min}$.

It follows from Eq. (66) that in the thin-wall regime, the radius R_c of the inner region (monopole-like core) is finite and does not depend on the phase frequency ω . In contrast, Eq. (68) tells us that the radius R of the intermediate region of the Q-ball type increases without bound as $|\omega| \rightarrow \omega_{\min}$. The energy and the Noether charge of the soliton are $\propto R^3$, and therefore they also increase without bound as $|\omega| \rightarrow \omega_{\min}$. The effective thickness of the outer region and the surface tension T are practically independent of the phase frequency ω and can be considered as constants. Finally, the long-range chromomagnetic field (38) of dipole type extends far beyond the outer region of the soliton.

B. The thick-wall regime

In the thick-wall regime, the magnitude of the phase frequency ω tends to a maximum value equal to m . In this regime, the effective potential (17) has a first-order zero located at $h_0 \approx m_\omega m^{-1}(1 + \varepsilon^2)^{1/2}$, where $m_\omega = (m^2 - \omega^2)^{1/2}$. We see that this zero is located in a small

neighborhood of $h = 0$, since m_ω is small in the thick-wall regime. The analysis of the system (15) – (16) based on the mechanical analogy [14] shows that the maximum value of the ansatz function $h(r)$ is of the order of h_0 , and hence is small. At the same time, the ansatz function $u(r)$ is not small and is of the order of unity. Finally, Eq. (34) tells us that the dimensionless combination $m_\omega r$ is natural in the thick-wall regime.

In the light of the above, we write the ansatz functions in the form $u(r) = \tilde{u}(\varrho)$ and $h(r) = m_\omega m^{-1} \tilde{h}(\varrho)$, where $\varrho = m_\omega r$. Using these expressions for the ansatz functions, we find that the Lagrangian can be written as

$$L = m_\omega \tilde{L}_1 + m_\omega^3 \tilde{L}_3, \quad (74)$$

where

$$\tilde{L}_1 = 4\pi v^2 \int_0^\infty \left[-\frac{2\tilde{u}'(\varrho)^2}{m_V^2 \varrho^2} - \frac{(\tilde{u}(\varrho)^2 - 1)^2}{m_V^2 \varrho^4} \right. \quad (75)$$

$$\left. - \frac{1}{2m^2} \tilde{h}'(\varrho)^2 - \frac{\tilde{h}(\varrho)^2 \tilde{u}(\varrho)^2}{m^2 \varrho^2} + \frac{1}{m^2} \tilde{W}(\tilde{h}(\varrho)) \right] \varrho^2 d\varrho,$$

$$\tilde{W}(\tilde{h}) = -\frac{\tilde{h}^2}{2} + \frac{1}{(1 + \varepsilon^2)} \frac{\tilde{h}^4}{2}, \quad (76)$$

and

$$\tilde{L}_3 = -4\pi v^2 \int_0^\infty \left[\frac{1}{8} \frac{\tilde{h}^6(\varrho)}{m^4 (1 + \varepsilon^2)} \right] \varrho^2 d\varrho. \quad (77)$$

Note that both \tilde{L}_1 and \tilde{L}_3 do not depend on ω .

In the thick-wall regime, the parameter $m_\omega = (m^2 - \omega^2)^{1/2}$ is small, and therefore we can neglect the second term in Eq. (74). Then by analogy with Eqs. (70) and (71), we obtain the expressions of the Noether charge and the energy of the soliton in the thick-wall regime

$$Q(\omega) = \frac{dL}{d\omega} = \omega (m^2 - \omega^2)^{-1/2} |\tilde{L}_1| \quad (78)$$

and

$$E(\omega) = \omega \frac{dL}{d\omega} - L(\omega) = m^2 (m^2 - \omega^2)^{-1/2} |\tilde{L}_1|. \quad (79)$$

Using Eqs. (78) and (79), we find that in the thick-wall approximation, the derivative $dE/dQ = \omega$, and the ratio

$$\frac{E}{Q} = \frac{m^2}{\omega}. \quad (80)$$

Thus, in the thick-wall regime $|\omega| \rightarrow m$, the amplitude of the ansatz function $h(r)$ tends to zero proportional to $m_\omega \approx (2m)^{1/2}(m - |\omega|)^{1/2}$. In addition, due to the combination $m_\omega r$ in the argument, the ansatz function $h(r) = m_\omega m^{-1} \tilde{h}(m_\omega r)$ spreads out in space. In contrast, $u(r)$ and $1 - u(r)$ remain of the order of unity. Both the energy and the magnitude of the Noether charge increase indefinitely $\propto (m - |\omega|)^{-1/2}$ as $|\omega| \rightarrow m$. This growth, however, is significantly weaker than in the thin-wall regime in which it is $\propto (|\omega| - \omega_{\min})^{-3}$.

V. NUMERICAL RESULTS

The system of differential equations (15) and (16) with the boundary conditions

$$\begin{aligned} u(0) &= 1, & \lim_{r \rightarrow \infty} u(r) &= 1, \\ h(0) &= 0, & \lim_{r \rightarrow \infty} h(r) &= 0, \end{aligned} \quad (81)$$

is a Dirichlet boundary value problem on the semi-infinite interval $r \in [0, \infty)$, which can be solved only by numerical methods. To solve this bvp problem, we used the numerical methods of the MAPLE package [19]. To check the correctness of the numerical solutions obtained, we used the virial relation (46) and the differential relation (49).

The bvp problem depends on the five parameters g , ω , m , v , and ε , while the ansatz functions $u(r)$ and $h(r)$ are dimensionless. Eqs. (15) and (16) tell us that these two functions depend on four dimensionless variables and can be written as $u(\rho, \tilde{\omega}^2, \kappa^2, \varepsilon)$ and $h(\rho, \tilde{\omega}^2, \kappa^2, \varepsilon)$, where $\rho = mr$, $\tilde{\omega} = \omega/m$, and $\kappa = m_V/m = \sqrt{2}gv/m$. Using this information and Eqs. (20) and (22), we find that the energy and the Noether charge of the soliton can be written as

$$E = \frac{v}{g} \tilde{E}(\tilde{\omega}^2, \kappa^2, \varepsilon) \quad (82)$$

and

$$Q = \frac{v}{mg} \tilde{Q}(\tilde{\omega}, \kappa^2, \varepsilon) \quad (83)$$

respectively. Note that the energy (Noether charge) is an even (odd) function of the phase frequency.

From the above, it follows that, in essence, the bvp depends nontrivially on the three dimensionless parameters $\tilde{\omega}$, κ , and ε . Furthermore, we see that the energy E is inversely proportional to the gauge coupling constant g . Hence, the Lagrangian L and the action $S_T = 2\pi\omega^{-1}L$ are also $\propto g^{-1}$. It follows that the semiclassical regime corresponds to the condition $g \ll 1$, which we shall assume to be satisfied.

The behavior of the ansatz function h is determined by Eq. (16). Except for the term $-2r^{-2}u^2h$, which decreases rapidly with an increase in r , this equation coincides with the one that describes the behavior of the amplitude of the complex scalar field of a Q-ball [15, 20]. Furthermore, the sixth-order effective potential \tilde{U}_ω entering Eq. (16) admits the existence of a series of Q-ball solutions. Besides the basic nodeless Q-ball solution, the effective potential admits an infinite sequence of excited Q-ball solutions with monotonically increasing number of radial zeros. Considering the above, we can assume that the model (1) has a basic soliton solution and a series of radially excited solutions.

Figure 1 shows the ansatz functions $h(\rho)$ and $u(\rho)$ for the nodeless and two nodal (excited) soliton solutions. The curves in Fig. 1 correspond to the dimensionless parameters $\tilde{\omega} = 0.7$, $\kappa = 1$, and $\varepsilon = 1/3$. To avoid clutter,

we limited ourselves to the two nodal solutions corresponding to $n = 2$ and 5. It follows from Fig. 1 that the spatial (radial) size of the soliton increases rapidly with an increase in the number of nodes n . This applies to both the central and nodal parts of the soliton. We also note that as the number of nodes increases, the central part of the soliton has a behavior specific to the thin-wall regime. In particular, the ansatz function $h(\rho)$ is approximately constant in the central region (except for the monopole-like core), and the ansatz function $u(\rho)$ is close to zero in most of the central and nodal regions.

According to Eq. (23), the ansatz function $u(\rho)$ determines the chromomagnetic field of the soliton. In particular, Eq. (23) tells us that the chromomagnetic field can be divided into longitudinal ($\propto n^a n^i$) and transverse ($\delta^{ai} - n^a n^i$) components. The values of the longitudinal and transverse components are determined by the scalar functions $B_{\parallel}(r) = (u(r)^2 - 1)/(gr^2)$ and $B_{\perp}(r) = u'(r)/(gr)$, respectively. In the case of the magnetic monopole, the longitudinal component determines the long-range ($\propto r^{-2}$) part of the magnetic field corresponding to an unbroken Abelian subgroup of a non-Abelian gauge group. At the same time, the transverse component is the short-range ($\propto \exp(-m_V r)$) part of the monopole's magnetic field corresponding to the broken part of the non-Abelian gauge group.

The isovector scalar field of the monopole is different from zero at large r , and therefore the gauge symmetry is broken there, and the transverse part of the monopole's magnetic field is exponentially suppressed compared to the longitudinal part. In contrast, the isovector scalar field of the nontopological soliton considered here vanishes exponentially at large r . As a result, the gauge symmetry is unbroken at large r , and both the longitudinal and transverse parts of the chromomagnetic field are long-range ($\propto r^{-3}$).

We define the dimensionless rescaled versions of B_{\parallel} and B_{\perp} as $\tilde{B}_{\parallel} = gm^{-2}B_{\parallel} = (u(\rho)^2 - 1)/\rho^2$ and $\tilde{B}_{\perp} = gm^{-2}B_{\perp} = u'(\rho)/\rho$, respectively. Figure 2 shows the curves $\rho^3 \tilde{B}_{\parallel}(\rho)$ and $\rho^3 \tilde{B}_{\perp}(\rho)$ for the nodeless and the first five nodal soliton solutions on a semilogarithmic scale. It also shows the curve $\rho^3 \tilde{B}_m(\rho)$, where $\tilde{B}_m(\rho) = -\rho^{-2}$ is the long-range Abelian magnetic field of the 't Hooft-Polyakov monopole. We see that $\tilde{B}_{\parallel}(\rho)$ and $\tilde{B}_{\perp}(\rho)$ behave quite differently in the inner region of the soliton, where the gauge symmetry is partially broken. $\tilde{B}_{\parallel}(\rho)$ corresponds to the unbroken $U(1)$ gauge subgroup, and therefore it is long-range ($\propto \rho^{-2}$) just like the Abelian part of the monopole's magnetic field. In contrast, similarly to the non-Abelian part of the monopole's magnetic field, $\tilde{B}_{\perp}(\rho)$ is exponentially suppressed in the inner region.

The situation changes in the external region, where the isovector scalar field vanishes and the gauge symmetry is restored. For this reason, both $\tilde{B}_{\parallel}(\rho)$ and $\tilde{B}_{\perp}(\rho)$ are long-range in this region. As ρ increases, the long-range character of $\tilde{B}_{\parallel}(\rho)$ changes from pole-like ($\propto \rho^{-2}$)

to dipole-like ($\propto \rho^{-3}$). The behavior of $\tilde{B}_\perp(\rho)$ also becomes dipole-like for sufficiently large ρ . Note that according to Eq. (38), the ratio $\tilde{B}_\parallel/\tilde{B}_\perp \rightarrow -2$ as $\rho \rightarrow \infty$.

Figure 3 shows the dependence of the rescaled Noether charge $\tilde{Q} = mv^{-1}gQ$ on the dimensionless phase frequency $\tilde{\omega} = m^{-1}\omega$ for the nodeless and the first five nodal soliton solutions. The curves in Fig. 3 and subsequent Figs. 4 – 6 correspond to the dimensionless parameters $\kappa = 1$ and $\varepsilon = 1/3$. We see that \tilde{Q} increases without bound as $\tilde{\omega}$ decreases, which corresponds to the transition to the thin-wall regime. It was found numerically that in this case, $\tilde{Q}(\tilde{\omega}) \propto (\tilde{\omega} - \tilde{\omega}_{\min})^{-3}$, where $\tilde{\omega}_{\min} = \varepsilon(1 + \varepsilon^2)^{-1/2} = 10^{-1/2}$. Such a behavior of the Noether charge \tilde{Q} is consistent with Eq. (70). The Noether charges of the soliton solutions also increase indefinitely when $\tilde{\omega} \rightarrow 1$, which corresponds to the transition to the thick-wall regime. In this case, the Noether charges $\tilde{Q}(\tilde{\omega}) \propto (1 - \tilde{\omega})^{-1/2}$, which is consistent with Eq. (78). It follows from Fig. 3 that at a fixed $\tilde{\omega}$, the Noether charge \tilde{Q} increases monotonically with an increase in the number of nodes n , and the rate of increase also grows with n . The behavior of the curves $\tilde{E}(\tilde{\omega})$ is similar to that presented in Fig. 3. In particular, the soliton's energy $\tilde{E} \rightarrow \infty$ both as $\tilde{\omega} \rightarrow \tilde{\omega}_{\min}$ and $\tilde{\omega} \rightarrow 1$.

Figure 4 presents the dependence of the ratio \tilde{E}/\tilde{Q} on \tilde{Q} for the nodeless and the first five nodal soliton solutions on a semilogarithmic scale. A characteristic feature of a curve in Fig. 4 is a cuspidal point that divides the curve into upper and lower branches. The presence of the cuspidal point is a typical sign of non-topological solitons [3, 16]. It follows from Fig. 4 that the Noether charge \tilde{Q} of a soliton reaches the minimum at this point. This is because the cuspidal point of a curve in Fig. 4 corresponds to the minimum point of the corresponding curve $\tilde{Q}(\tilde{\omega})$ in Fig. 3. Furthermore, Eq. (49) tells us that the energy of the soliton also reaches the minimum at the cuspidal point.

In Fig. 4, each curve intersects the line $\tilde{E}/\tilde{Q} = 1$ at a single point lying on the lower branch. In addition, the upper branch of each curve tends to unity from above as $\tilde{Q} \rightarrow \infty$. The value of the ratio $\tilde{E}/|\tilde{Q}|$ is a stability criterion for a soliton of the Noether charge \tilde{Q} to the transition into a plane-wave configuration with the same Noether charge. In the dimensionless units used, the energy of the plane-wave configuration at rest is $\tilde{E}_{\text{pw}} = |\tilde{Q}|$, and therefore the ratio $\tilde{E}_{\text{pw}}/|\tilde{Q}| = 1$. It follows that the soliton stable (unstable) to the transition into the plane-wave configuration, provided that the ratio $\tilde{E}/|\tilde{Q}|$ is less (more) than unity. Hence, the upper branches of the curves correspond to unstable solitons as well as those parts of the lower branches for which $\tilde{E}/\tilde{Q} > 1$.

We continue our discussion on the stability of the soliton solutions. In addition to the transition (decay) into a plane-wave configuration, a soliton can also transition into another soliton with lower energy, the energy released being carried away by radiation. It follows from Fig. 4 that at a fixed \tilde{Q} , the energy \tilde{E} increases monotonically

with an increase in the number of nodes n . This applies to both the upper and the lower branches of the curves. Hence, a soliton with large n can transition into a soliton with smaller n , provided that the Noether charge of the final state (including that carried away by radiation) is equal to the Noether charge of the initial soliton.

It follows from Fig. 4 that for a given \tilde{Q} , the nodeless ($n = 0$) soliton of the lower branch of the \tilde{E}/\tilde{Q} curve has the lowest energy. The soliton solutions considered here are spherically symmetric modulo a global gauge transformation. In general, spherically symmetric solutions have lower energy than other solutions of the same \tilde{Q} . We can therefore assume that the nodeless soliton solutions of the lower branch are stable, provided that the ratio $\tilde{E}/\tilde{Q} < 1$. All other solitons are unstable. The instability can be either classical (unstable mode (modes) in the spectrum of fluctuation) or quantum-mechanical (tunnelling process). It was shown in [3] that a cuspidal point on a $\tilde{E}(\tilde{Q})$ curve means the appearance of an unstable fluctuation mode on the upper branch of the curve. Hence, in Fig. 4, the upper branches of all the curves correspond to classically unstable solitons. In addition, it was shown in [16] that radial nodes lead to classical instability of soliton solutions. We can therefore expect that the lower branches of the curves for which $n > 0$ also correspond to classically unstable solitons.

The lower branch of the $n = 0$ curve corresponds to classically stable solitons. However, the part of this lower branch in the vicinity of the cuspidal point is unstable to the transition into the plane-wave configuration because for this part, the ratio $\tilde{E}/\tilde{Q} > 1$. Given the above, we conclude that this part of the lower branch corresponds to the solitons that are unstable in the quantum-mechanical sense. The transition of these solitons into the plane-wave configuration is realized via tunneling. It should be noted that a similar situation (classically stable but quantum-mechanically unstable part of the $\tilde{E}(\tilde{Q})$ curve) also takes place for Q-balls [3, 16, 20].

Figure 5 shows the dependence of the ratio \tilde{E}/\tilde{Q} on the phase frequency $\tilde{\omega}$ for the nodeless and the first five nodal soliton solutions. It also shows a dashed curve that corresponds to the thin-wall regime and is described by Eq. (72). The cuspidal points of the curves in Fig. 4 correspond to the maximum points of the curves in Fig. 5. As in Fig. 4, each curve in Fig. 5 intersects the line $\tilde{E}/\tilde{Q} = 1$ at a single point, and all these curves tend to unity from above as $\tilde{\omega} \rightarrow 1$. This corresponds to the thick-wall regime and is in agreement with Eq. (80). As the phase frequency $\tilde{\omega}$ decreases, the soliton enters the thin-wall regime in which the ratio \tilde{E}/\tilde{Q} is determined by Eq. (72). It follows from Fig. 5 that in this regime, all the curves merge with the dashed curve. Hence, we conclude that as $\tilde{\omega}$ decreases, the behavior of the solitons is well described within the thin-wall approximation.

A characteristic feature of the studied solitons is the long-range dipole ($\propto r^{-3}$) chromomagnetic field. Eq. (37) tells us that the soliton's chromomagnetic dipole moment is determined by the parameter b , which also

determines the long-range ($\propto r^{-1}$) asymptotics of the ansatz function $u(r)$. We define the dimensionless version of b by $\tilde{b} = mb$ and recall that b is negative. In Fig. 6, we can see the graphs of $-\tilde{b}(\tilde{Q}^{1/3})$ for the nodeless and the first five nodal soliton solutions. The choice of $\tilde{Q}^{1/3}$ as an argument is because according to Eqs. (68) and (70), the effective radius R of the soliton is $\propto Q^{1/3}$ in the thin-wall regime.

Each curve in Fig. 6 has two branches which have a self-intersection point when the number of nodes $n = 0$ or 1. As \tilde{Q} increases, the lower (upper) branch goes to the thin-wall (thick-wall) regime in which $-\tilde{b}$ increases indefinitely. It was found numerically that the lower branches of the curves $-\tilde{b}(\tilde{Q}^{1/3})$ are asymptotically linear in $\tilde{Q}^{1/3}$. It follows that in the thin-wall regime, b is proportional to the effective soliton radius R .

In contrast, the upper branches of $-\tilde{b}(\tilde{Q}^{1/3})$ are asymptotically cubic in $\tilde{Q}^{1/3}$, i.e. they are asymptotically $\propto \tilde{Q}$ in the thick-wall regime. In this regime, the soliton spreads unboundedly through space, and its boundaries become blurred. In this case, according to Subsection IV B, the parameter $m_\omega^{-1} = (m^2 - \omega^2)^{-1/2}$ can be taken as an estimate of the size of the soliton. At the same time, Eq. (78) tells us that in the thick-wall regime, the Noether charge Q is also proportional to m_ω^{-1} . Summarising these facts, we conclude that in the thick-wall regime, b is proportional to the effective soliton radius. We see that in both extreme regimes, the chromomagnetic dipole moment is proportional to the soliton's linear size, which was to be expected on the basis of dimensional considerations.

VI. CONCLUSION

We have investigated a nontopological soliton of a non-Abelian gauge model. This model has similarities with the well-known $SU(2)$ Georgi-Glashow model while differing from it in three important aspects. First, the real scalar isotriplet of the Georgi-Glashow model is replaced by a complex scalar isotriplet. The transition to the complex scalar isotriplet results in a new global $U(1)$ symmetry and a corresponding Noether charge. Second, unlike the Georgi-Glashow model, the self-interaction potential of the considered model has a global minimum at zero value of the scalar isotriplet, and therefore the $SU(2)$ gauge symmetry is not spontaneously broken. Third, the self-interaction potential of the Georgi-Glashow model is of the fourth order in the field, and therefore the model is renormalizable. At the same time, the self-interaction potential of the considered model is of the sixth order in the field, and its form coincides with that used in the study of Q-balls.

The above differences make possible the existence of a nontopological soliton in the framework of the model (1). Many properties of this soliton coincide with those of a Q-ball. These include a cuspidal point on the $E(Q)$

curve, the presence of the two (thin-wall and thick-wall) limiting regimes, and the existence of radially excited nodal solutions. A characteristic property of the soliton bringing it closer to a magnetic monopole is its spherically symmetric magnetic field. In the thin-wall regime, the magnetic field of the soliton in the inner region practically coincides with that of a magnetic monopole. In particular, in the inner region of the soliton, the Abelian component of the magnetic field $B_i \approx n_i/(gr)^2$, while the non-Abelian component is suppressed exponentially.

The situation changes in the external region, where the scalar field vanishes and the non-Abelian gauge symmetry is restored. In this region, the Abelian component of the magnetic field has the asymptotics of dipole ($\propto r^{-3}$) type, which means zero magnetic charge of the soliton. Moreover, in this region, the other components of the magnetic field also have long-range dipole ($\propto r^{-3}$) asymptotics. Thus, at large distances from the center, the soliton possesses a long-range chromomagnetic field of dipole type. For the two (thin-wall and thick-wall) limiting regimes, the chromomagnetic dipole moment of the soliton is proportional to its linear size.

We can say that the nontopological soliton is composed of a monopole-like core surrounded by a Q-ball-like shell. This shell completely shields the magnetic charge of the core, which results in the dipole ($\propto r^{-3}$) magnetic field of the soliton at a large distance from the center. Just like the usual Q-ball, the size of the shell increases indefinitely as $\tilde{\omega} \rightarrow \tilde{\omega}_{\min}$ (thin-wall regime).

Having a long-range chromomagnetic field, the soliton nevertheless possesses a zero electric field. This is because in the model (1), any spherically symmetric field configurations with a non-zero electric field will have infinite energy. In contrast, there exist electrically charged magnetic monopoles (dyons) which have finite energy [21]. In this connection it is worth noting that at large distances from the dyon, the non-Abelian gauge symmetry is broken except for the electromagnetic Abelian $U(1)$ subgroup. Hence, the long-range electric field of the dyon is Abelian. However, the non-Abelian gauge symmetry is not broken at large distances from the soliton of the model (1). It follows that if the soliton could have a long-range electric field it would be non-Abelian (chromoelectric) like its chromomagnetic field.

It is worth noting that there are also no magnetic monopoles (chromodyons) possessing a long-range chromoelectric field [22–27]. The reason is that the long-range tails of the non-Abelian components of the fields produce a topological obstruction that makes it impossible to find a basis for an unbroken non-Abelian subgroup that is smooth over all of space. As a result, it is impossible to define normalizable zero modes which would correspond to some generators of the unbroken gauge non-Abelian subgroup.

The nontopological soliton considered here is related to the gauged monopole-bubble solution of [13]. Unlike the model (1), the model considered in [13] contains a real isovector scalar field, so that the conserved Noether

charge (22) is absent. In addition, the true vacuum manifold of this model is a two-sphere $|\phi| = \phi_{\text{vac}}$ rather than the point $\phi = 0$ as it is in the model (1). We can say that the gauged monopole-bubble of [13] and the non-topological soliton of the model (1) are related similarly to the three-dimensional Euclidean bounce and the (3+1) dimensional Q-ball. The gauged monopole-bubble contributes to the decay amplitude of a false vacuum in the high-temperature limit.

The model of [13] and the model (1) can be regarded as modifications of the $SU(2)$ Georgi-Glashow model [6]. Another modification was considered in [7, 8]. The effective self-interaction potentials used in [7, 8] result in a true vacuum at the zero point $\phi = 0$ and a false vacuum manifold on the two-sphere $|\phi| = \phi_{\text{vac}}$. It was shown in [7, 8] that a metastable topological soliton,

called the false monopole, exists in that model. This name stems from the fact that the real isovector scalar field of this soliton approximates the false vacuum manifold $|\phi| = \phi_{\text{vac}}$ at large distances from the center. This false vacuum can decay via the usual creation of true vacuum bubbles [14]; however, it was shown in [7–12] that this decay can be considerably enhanced in the presence of the false monopoles.

ACKNOWLEDGMENTS

This work was supported by the Russian Science Foundation, grant No 23-11-00002.

-
- [1] N. Manton and P. Sutcliffe, *Topological Solitons* (Cambridge University Press, Cambridge, 2004).
 - [2] E. J. Weinberg, *Classical Solutions in Quantum Field Theory: Solitons and Instantons in High Energy Physics* (Cambridge University Press, Cambridge, 2012).
 - [3] T. D. Lee and Y. Pang, Phys. Rep. **221**, 251 (1992).
 - [4] G. 't Hooft, Nucl. Phys. B **79**, 276 (1974).
 - [5] A. M. Polyakov, JETP Lett. **20**, 194 (1974).
 - [6] H. Georgi and S. L. Glashow, Phys. Rev. D **6**, 2977 (1972).
 - [7] B. Kumar, M. B. Paranjape, and U. A. Yajnik, Phys. Rev. D **82**, 025022 (2010).
 - [8] M. B. Paranjape and Y. Saxena, Phys. Rev. D **110**, 025005 (2024).
 - [9] P. J. Steinhardt, Phys. Rev. D **24**, 842 (1981).
 - [10] P. J. Steinhardt, Nucl. Phys. B **190**, 583 (1981).
 - [11] Y. Hosotani, Phys. Rev. D **27**, 789 (1983).
 - [12] P. Agrawal and M. Nee, SciPost Phys. **13**, 049 (2022).
 - [13] Y. Kim, S. Lee, K. Maeda, and N. Sakai, Phys. Lett. B **452**, 214 (1999).
 - [14] S. Coleman, Phys. Rev. D **15**, 2929 (1977).
 - [15] S. Coleman, Nucl. Phys. B **262**, 263 (1985).
 - [16] R. Friedberg, T. D. Lee, and A. Sirlin, Phys. Rev. D **13**, 2739 (1976).
 - [17] A. Yu. Loginov, Phys. Lett. B **822**, 136662 (2021).
 - [18] A. Yu. Loginov, Phys. Lett. B **855**, 138840 (2024).
 - [19] Maple 2022.1, Maplesoft, a division of Waterloo Maple Inc., Waterloo, Ontario.
 - [20] F. P. Correia and M. Schmidt, Eur. Phys. J. C **21**, 181 (2001).
 - [21] B. Julia and A. Zee, Phys. Rev. D **11**, 2227 (1975).
 - [22] A. Abouelsaood, Nucl. Phys. B **226**, 309 (1983).
 - [23] A. Abouelsaood, Phys. Lett. B **125**, 467 (1983).
 - [24] A. Balachandran, G. Marmo, N. Mukunda, J. Nilsson, E. Sudarshan, and F. Zaccaria, Phys. Rev. Lett. **50**, 1553 (1983).
 - [25] P. Nelson, Phys. Rev. Lett. **50**, 939 (1983).
 - [26] P. Nelson and A. Manohar, Phys. Rev. Lett. **50**, 943 (1983).
 - [27] P. Nelson and S. Coleman, Nucl. Phys. B **237**, 1 (1984).

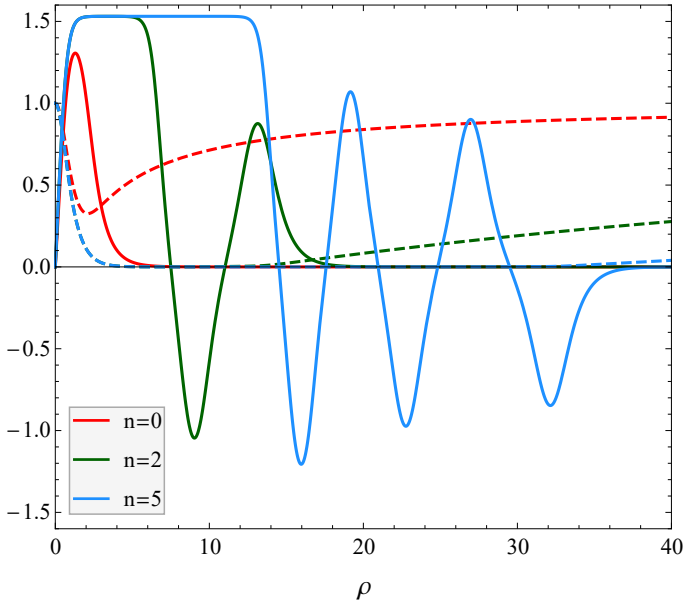


FIG. 1. The ansatz functions $h(\rho)$ (solid curves) and $u(\rho)$ (dashed curves) for the nodeless ($n = 0$) and two nodal ($n = 2$ and 5) soliton solutions.

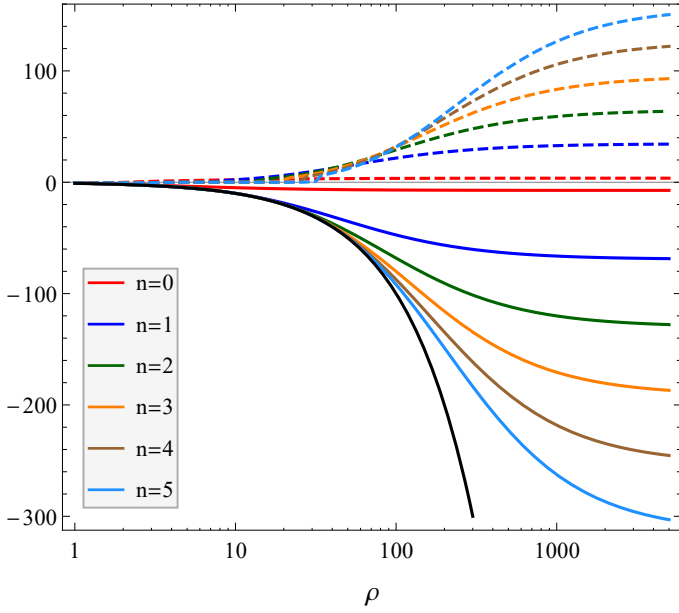


FIG. 2. The curves $\rho^3 \tilde{B}_{||}(\rho)$ (solid) and $\rho^3 \tilde{B}_{\perp}(\rho)$ (dashed) for the nodeless and the first five nodal soliton solutions. The black solid curve corresponds to $\rho^3 \tilde{B}_m(\rho)$, where $\tilde{B}_m(\rho) = -\rho^{-2}$ is the long-range Abelian magnetic field of the 't Hooft-Polyakov monopole.

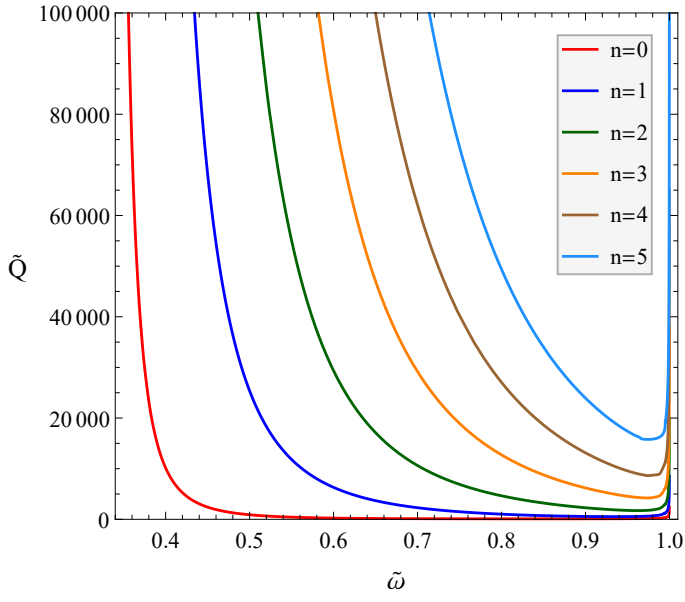


FIG. 3. The curves $\tilde{Q}(\tilde{\omega})$ for the nodeless and the first five nodal soliton solutions.

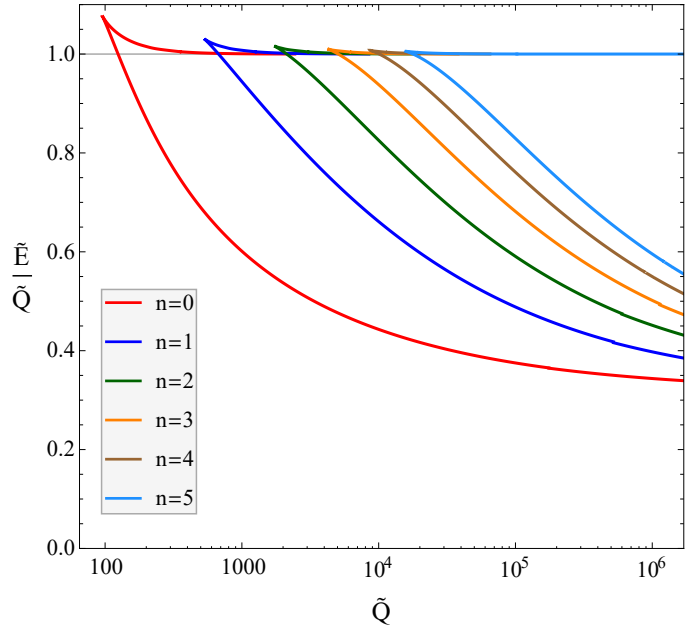


FIG. 4. Dependence of the ratio \tilde{E}/\tilde{Q} on \tilde{Q} for the nodeless and the first five nodal soliton solutions.

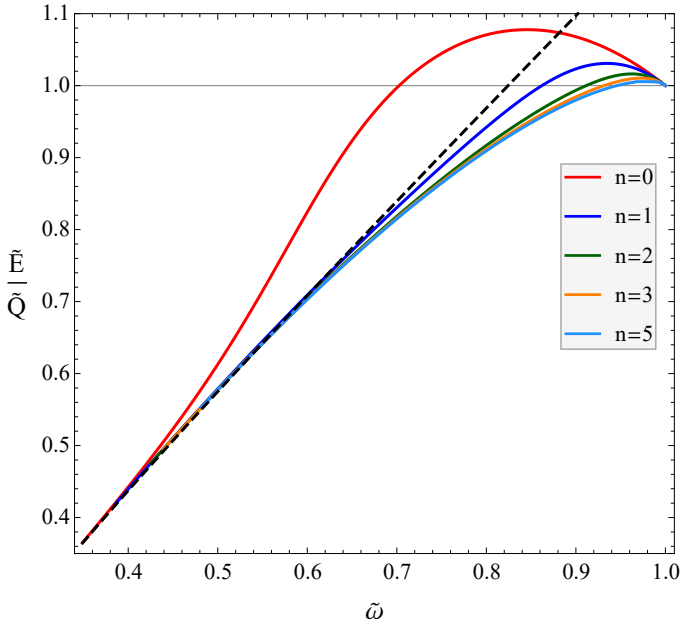


FIG. 5. Dependence of the ratio \tilde{E}/\tilde{Q} on $\tilde{\omega}$ for the nodeless and the first five nodal soliton solutions. The curve for $n = 4$ is visually indistinguishable from the curve for $n = 5$. The black dashed curve corresponds to Eq. (72).

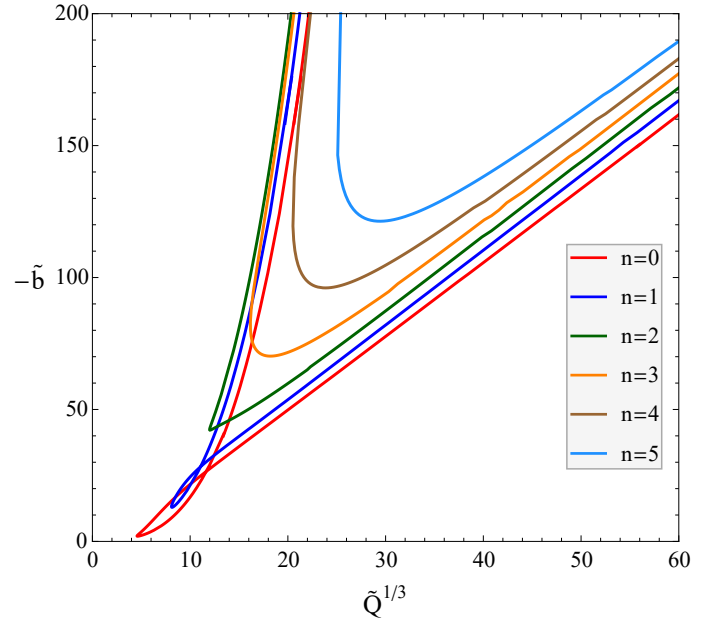


FIG. 6. The curves $-\tilde{b}(\tilde{Q}^{1/3})$ for the nodeless and the first five nodal soliton solutions.